Assessment of Fault Crossing Effects on a Seismically Isolated Multi-Span Bridge

A. Ucak & G.P. Mavroeidis
The Catholic University of America, USA

P. Tsopelas
University of Thessaly, Greece

SUMMARY:
In this paper, the effect of fault crossing on the seismic response of a multi-span seismically isolated bridge (Bolu Viaduct) is investigated. First, the seismic ground motions at the site of the Viaduct are generated following a rigorous methodology. Then, the generated motions are used to study the effect of fault crossing on the nonlinear behaviour of the seismically isolated multi-span bridge. The spatially varying ground motion due to fault crossing is accounted for in the study. It is shown that fault crossing is an important factor in the earthquake response of seismically isolated bridges, and that this effect needs to be considered in the design and detailing of the isolation system.

Keywords: Fault crossing, synthetic ground motion, seismic isolation, Bolu Viaduct

1. INTRODUCTION

The Duzce earthquake struck a segment of the North Anatolian Fault in western Turkey on November 12, 1999. It had a magnitude of M_w 7.2 and occurred just eastward of the M_w 7.4 Izmit earthquake of August 17, 1999. The hypocenter was located at (40.82^{o}N, 31.186^{o}E), according to the Kandilli Observatory, and at depth of 12 km.

The structure under consideration in this study, Bolu Viaduct 1, is located in central Turkey. It is a small but very important segment of the Trans-European Motorway, connecting Turkey's capital Ankara to Istanbul. The 2.3km long viaduct consists of 59 dual spans, each being approximately 40m long. The original design of the superstructure called for seven lines of simply supported pre-stressed concrete box girders for each span and a slab that was continuous over a segment of 10 spans. Each segment consisted of 11 hollow core concrete piers with varying heights and a plan dimension of 4.5x8 m, resting on massive 3m thick pile caps. The foundation system consisted of a 4x3 pile group consisting of 1.8m diameter cast-in-drilled-hole piles that pass tough soil with variable strength (Roussis et al. 2003). Reconnaissance reports suggest that during the 1999 Duzce earthquake, the fault crossed the westbound carriageway of the viaduct between piers P46 and P47, and the eastbound carriageway of the viaduct between peers P44 and P45, at an angle of approximately 25° measured with respect to the longitudinal direction of the viaduct (Roussis et al. 2003, Park et al. 2004).

In the original design, a seismic isolation system consisting of lubricated flat sliders together with steel yielding devices was utilized. The isolation system and the viaduct were severely damaged during the 1999 Duzce earthquake due to inadequate design and inadequate size of the steel yielding devices (Roussis et al. 2003). After the earthquake, the structure was retrofitted such that (a) the superstructure (i.e., box girders and deck slab) was made continuous over the 10 span segment, and (b) each pier top was equipped with two large capacity friction pendulum bearings (FPS), providing restoring force through the curvature of the sliding interface and energy dissipation through friction (Ucak and Tsopelas 2007).

The earthquake ground excitation was recorded by three strong motion instruments (i.e., DZC, BOL, GOL) deployed in the source region. However, none of these instruments was located in the immediate vicinity of the Bolu Viaduct. Therefore, the intensity, duration and frequency content of the ground shaking that the viaduct sustained during the earthquake were not measured instrumentally. Furthermore, the ground motions recorded at DZC, BOL and GOL stations are not characterized by intense pulse-like motions that are typical of near-fault seismic excitations (see e.g., Mavroeidis and Papageorgiou 2003), and therefore are not deemed appropriate for the assessment of the seismic performance of the Bolu Viaduct, which was crossing the Duzce fault.

Researchers have attempted to estimate the ground motion in the vicinity of the viaduct in order to investigate and interpret the observed structural damage. Roussis et al. (2003) utilized a deterministic approach to simulate the ground motion in the low-frequency range and a stochastic approach to simulate the high-frequency components of ground motion. For the low-frequency components, a moving ramp-type dislocation function (Luco and Anderson 1983) with a maximum displacement of 5.6m and a rise time of 1s were considered. The compressional and shear wave velocities, as well as the rupture velocity were assumed to be constant, and the causative fault plane was assumed to be vertical with a width of 18km. The simulation of the high-frequency content of the ground motion was based on a stochastic approach utilizing the following parameters: M_w=7.2, fault distance of 1km, and good soil conditions.

Park et al. (2004) employed a fast and efficient method to generate broadband ground motions in the vicinity of the Bolu Viaduct by combining a recorded far-field ground motion record with simple pulses that portray near-fault features. The BOL record was selected as the far-field ground motion, while the directivity and permanent translation (fling) pulses were approximated analytically using the simple trigonometric functions of Makris and Chang (2000).

The main objectives of this paper are: (a) to generate seismic motions at the site of the Bolu Viaduct using a rigorous methodology; (b) to explain the failure of the original design of the isolation system of the Bolu Viaduct utilizing the rigorously generated seismic excitations; and (c) to study the effects of fault crossing on the seismically isolated Bolu Viaduct.

2. SIMULATION OF GROUND MOTION AT BOLU VIADUCT LOCATION

In this section, broadband ground motions are generated at the location of the Bolu Viaduct by using a hybrid simulation approach which is based on physical models of the extended seismic source. The low-frequency ground motion is simulated using the discrete wavenumber representation method (Bouchon and Aki, 1977; Bouchon, 1979), while the high-frequency ground motion is simulated using the specific barrier model (Papageorgiou and Aki, 1983a,b).

2.1. Faulting Model

Several investigators have studied the fault rupture process of the Duzce earthquake and inferred the slip distribution on the causative fault by performing inversion analyses of teleseismic, strong motion, InSAR, and/or GPS data. The faulting model proposed by Bouin et al. (2004) is used in the present study. It was inferred from a joint inversion of GPS measurements and strong motion data recorded at DZC, BOL, SKR and GOL stations. The model provides tomographic images of the rupture front and slip duration, alongside the distributions of strike-slip and dip-slip offsets on the causative fault plane. The model consists of a single segment which is 40km long and 20km wide starting at the earth's free surface. The fault strike and dip angles are 265^o and 65^o NW, respectively.

2.2. Low-Frequency Ground Motion Simulation

The computation of the low-frequency ground motion is carried out using the discrete wavenumber representation method (Bouchon and Aki, 1977; Bouchon, 1979). The fault fracture is modeled as an ensemble of extended dislocation sources with rupture properties (e.g., slip, rise time, rupture velocity) consistent with the faulting model proposed by Bouin et al. (2004). The generalized transmission and reflection coefficient technique (Luco and Apsel 1983) is utilized for the propagation of the wavefield through the layered halfspace. The one-dimensional simplified crustal model of Bouin et al. (2004) is also used in the present study for the low-frequency simulations.

Since the idealized rectangular fault plane from the inversion analysis does not intersect the Bolu Viaduct at Pier 45, the low-frequency synthetic ground motion is generated at a representative location in the vicinity of the viaduct (i.e., southward to the intersection of the upper edge of the idealized fault plane with the viaduct). Figure 1 illustrates the time histories of the low-frequency (i.e., $0<f<2.5$Hz) acceleration, velocity and displacement components over a time window of 50s. The horizontal components are oriented along the North-South (N-S) and East-West (E-W) directions.

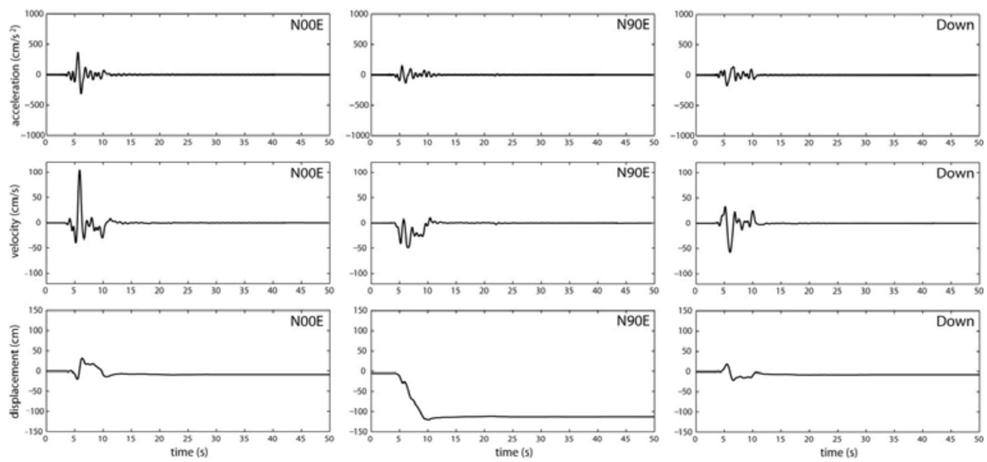

Figure 1. Low-frequency ground acceleration, velocity and displacement components (i.e., N-S, E-W and vertical, from left to right) generated using the discrete wavenumber representation method.

The ground motion component along the N-S direction (which approximately coincides with the fault-normal direction) is characterized by an intense forward-directivity pulse as evident from the velocity and acceleration time histories. The amplitude of the ground velocity pulse is approximately 100cm/s, a value which is in agreement with the typical slip velocity value of 100cm/s frequently considered by seismologists. The ground motion component along the E-W direction (which approximately coincides with the fault-parallel direction) is affected by the permanent translation (fling) effect as evident from the displacement time history. According to Akyuz et al. (2002), Pucci et al. (2007) and Guney et al. (2010), the magnitude of the ground dislocation in the fault-parallel direction across the rupture was approximately 1.5-2.0m in the vicinity of the viaduct, which implies a static displacement of 0.75-1.0m in opposite directions on the opposite sides of the surface rupture. Therefore, the static displacement of 1.1m towards west obtained in the present study is consistent with the upper bound of the permanent tectonic offset measured in the area after the earthquake.

2.3. High-Frequency Ground Motion Simulation

The computation of the high-frequency ground motion is carried out using the specific barrier model (Papageorgiou and Aki 1983a,b). The model applies both in the “near-field” and “far-field” regions, allowing for consistent ground motion simulations over the entire frequency range and for all distances of engineering interest. In the model, the fault is visualized as an ensemble of non-overlapping circular subevents of equal diameter that cover a rectangular fault. As the rupture front sweeps the fault plane with a sweeping velocity, a local stress drop occurs on each subevent. The subevent rupture starts from its center and spreads radially with a constant spreading velocity. The specific barrier model has been calibrated to shallow crustal earthquakes of three different tectonic regions: interplate, intraplate, and extensional regimes (Halldorsson and Papageorgiou 2005). Given an earthquake magnitude and the tectonic region, the interdependence of other source parameters on the local stress drop and the barrier interval allows the causative earthquake fault to be constructed. The calibrated specific barrier model (Halldorsson and Papageorgiou 2005) is used in the present study to simulate the high-frequency ground motion in the vicinity of the Bolu Viaduct. Figure 2 illustrates the high-frequency (i.e., f>0.2Hz) acceleration, velocity and displacement time histories assuming a NEHRP site class D characterization.

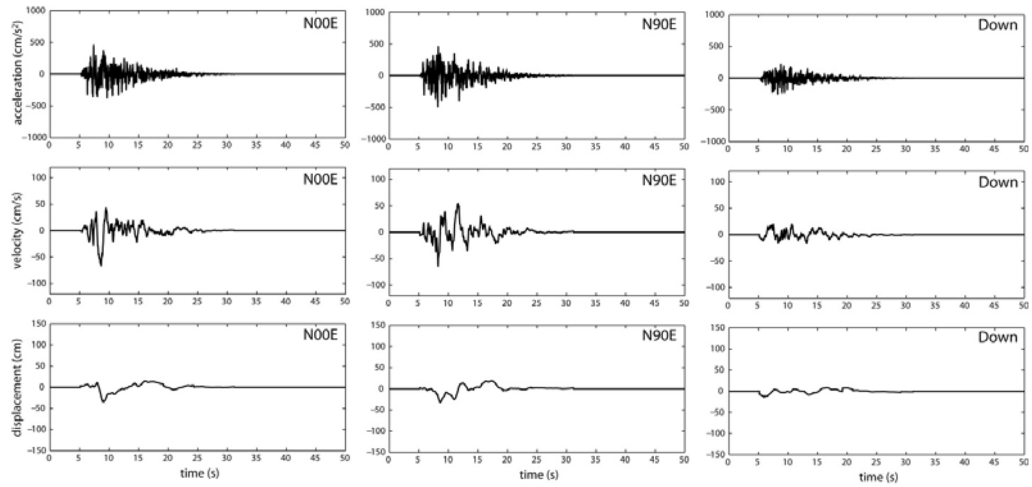

Figure 2. High-frequency ground acceleration, velocity and displacement components generated using the specific barrier model.

2.4. Broadband Motions

Figure 3 displays the broadband acceleration, velocity and displacement time histories in the vicinity of the Bolu Viaduct obtained by combining the results of low- and high-frequency simulations using matched filtering at a crossover frequency of 1Hz. It appears that the peak horizontal ground acceleration which the viaduct sustained during the 1999 Duzce earthquake was of the order of 0.5g, while the duration of the ground excitation was approximately 25s. The obtained PGA value is in good agreement with the range of PGA values reported by Ugurhan and Askan (2010) for the same region due to the Duzce earthquake.

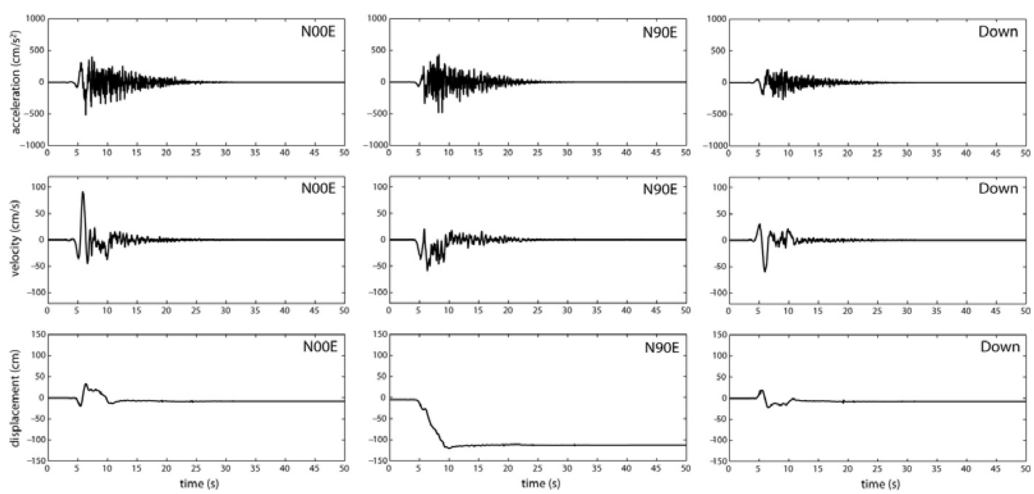

Figure 3. Broadband ground acceleration, velocity and displacement time histories generated by combining the low- and high-frequency simulation results.

As was mentioned previously, the synthetic ground motions have been generated for a representative site in the vicinity of the Bolu Viaduct, southward to the intersection of the upper edge of the idealized fault plane with the viaduct (see Fig. 6). Since the Duzce fault crosses the Viaduct at an angle of 25^o, it is also necessary to generate synthetic ground motions on the opposite side of the surface rupture (i.e., northward to the intersection of the fault with the viaduct). Figure 4 illustrates pairs of synthetic horizontal ground motions on opposite sides of the fault rupture. The ground motions for Side I (south) were obtained by simply rotating the horizontal ground motion components of Fig. 3 to the fault-normal and fault-parallel directions. The fault-normal component for Side II (north) was assumed to be identical to the fault-normal component for Side I in order to ensure kinematic continuity in the fault-normal direction. To account for the ground dislocation in the fault-parallel direction across the rupture, the fault-parallel component for Side II was assumed to be equal in magnitude to the fault-parallel component for Side I but with a reversed polarity. These assumptions are accurate because the central and eastern parts of the Duzce fault experienced almost pure right-lateral strike slip during the earthquake (see also e.g., Park et al. 2004 and Dreger et al. 2011). Finally, Fig. 5 illustrates the time histories of the synthetic ground motions of Fig. 4 rotated in the longitudinal and transverse directions of the Bolu Viaduct. These motions are subsequently used for the assessment of the seismic response of the Bolu Viaduct to the 1999 Duzce earthquake.

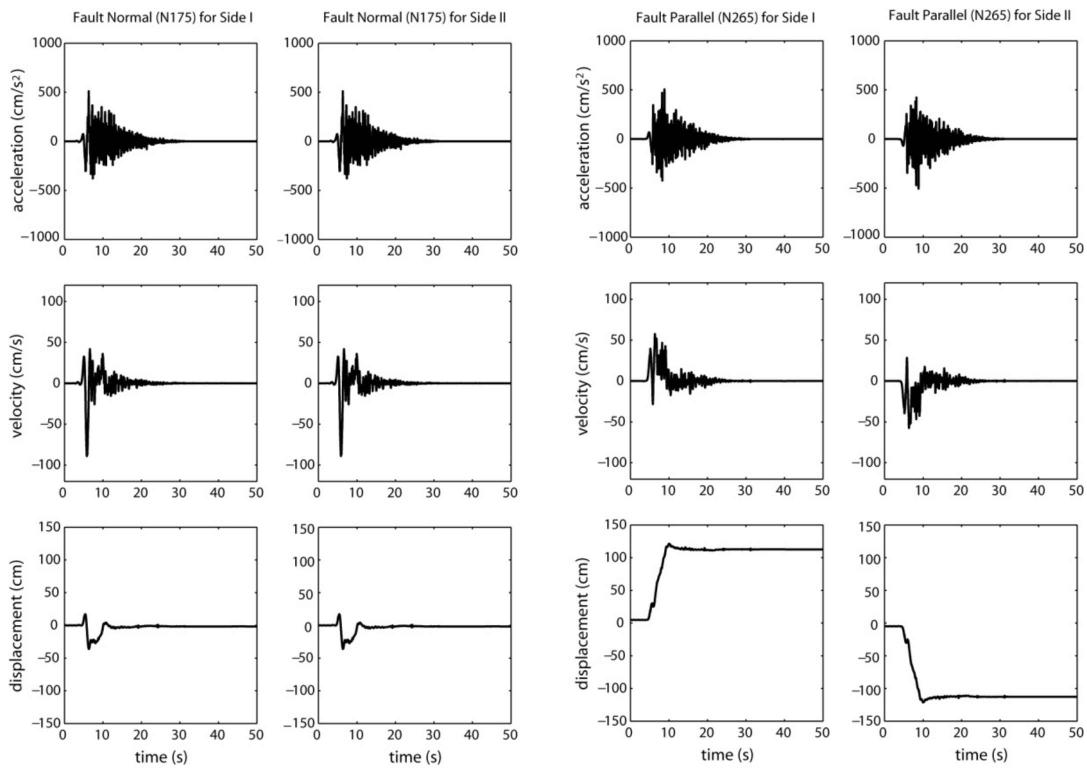

Figure 4. Fault-normal and fault-parallel components of acceleration, velocity and displacement time histories for sites located on either side of the fault trace (Side I: South, Side II: North).

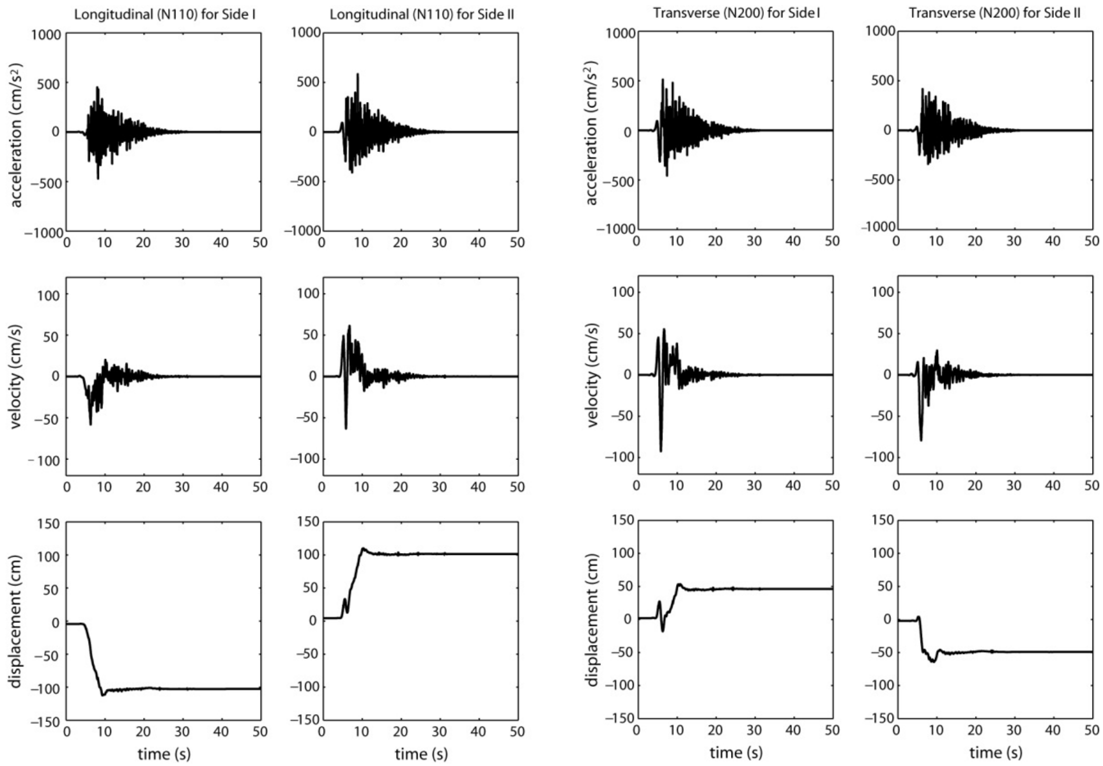

Figure 5. Longitudinal and transverse components of acceleration, velocity and displacement time histories for sites located on either side of the fault trace (Side I: South, Side II: North).

3. ANALYSES RESULTS OF A BOLU VIADUCT SEGMENT

Nonlinear time history analyses were carried out with the simulated ground motions of the 1999 Duzce earthquake, to determine the dynamic response and performance of a typical segment of the Bolu Viaduct (Fig. 6) as originally designed (and built). The finite element analyses were carried out using the commercially available finite element software Abaqus/Standard (2004). The model used in this study is based on the model utilized by Roussis et al. (2003). The interested reader is referred to Roussis et al. (2003) for further details and modeling parameters.

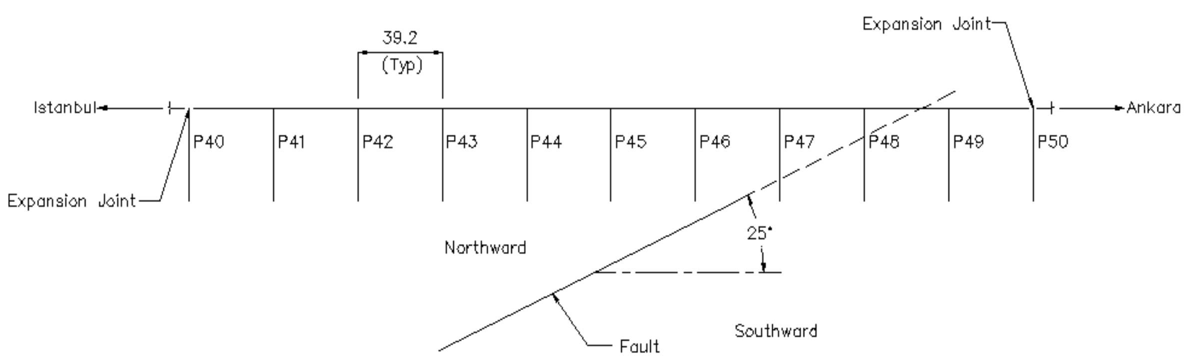

Figure 6. Schematic presentation of the analyzed viaduct segment.

The simulated ground motions shown in Fig. 5 (rotated in the longitudinal and transverse direction of the viaduct) were applied along the two orthogonal axes of the structure. The first analyses set, in which the bridge is assumed to be located next to the fault and excited by a spatially uniform ground motion, is named “Case A”. The scenario of “Case A” represents the design and analysis practice, where all the piers are excited at their bases with the same ground motion time history, that is, with the viaduct longitudinal and transverse motions simulated on the south side of the viaduct (Fig. 5 Side II). “Case B” is the second analyses set, in which the bridge is assumed to cross the fault and excited by a spatially varying ground motion. In “Case B”, piers P40 through P46 are excited with the viaduct longitudinal and transverse motions simulated on the north side (Fig. 5, Side II), while the remaining piers are excited with the ground motions simulated on the south side of the viaduct (Fig. 5, Side I).

The displacement time histories at the pier top, deck and isolation system at Pier 46, for “Case A” type analyses are presented in Fig. 7. The trace of the isolation displacement is also presented in the same figure. The displacement of the isolation system is the relative displacement between the deck and the pier top. The response histories for the remaining piers are similar, and not presented for brevity. It is important to note that “Case A” is the conventional design method, which assumes that the bridge is located next to the fault.

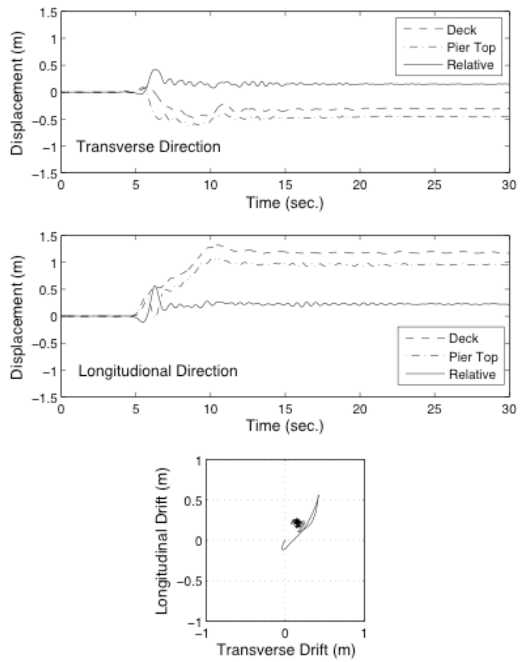

Figure 7. The displacement time histories computed at the deck, pier top and isolation system at Pier 46 for “Case A” type analysis (ignoring fault crossing).

An investigation of the displacement time histories shows that the response observed at the pier top and the deck is very similar to the input displacement. In the longitudinal direction, where a large fault permanent displacement is observed, there is very little relative deformation between the deck and pier top compared with the ground displacement. It appears that the isolation systems are not excited and the whole structure moves or displaces together with the ground. The forward-directivity pulse, which excited the structure, resulted in approximately 27cm isolation system permanent displacement.

For the original isolation system the maximum deformation demand computed is approximately 770mm (at Pier 50). The computed demand with the rigorously simulated seismic motion is far higher than the sliding bearing capacity (210mm), the steel-yielding devices capacity (480mm), and the design displacement considered (320mm) (Roussis et al. 2003). In addition, the computed demand is far below the relative displacement between the deck and pier top the viaduct experienced during the 1999 Duzce earthquake (Roussis et al. 2003). This discrepancy can be attributed to the fact that “Case A” analyses ignore the fault crossing, and the differential ground displacement at the fault.

Figure 8 depicts the deck, pier top and isolation displacement time history responses for “Case B” type analyses, at Piers 46 and 47. Piers 46 and 47 are located at the left and right side of the fault. It is important to note that in “Case B” the differential ground displacement between the two sides of the fault is accounted for, something which is usually ignored during the design face where the engineers utilize some “near-fault” excitations from publicly accessed databases and perform the “Case A” type of analyses to obtain design displacements.

A comparison of the results presented in Fig. 8 with the ones given in Fig. 7 shows that the computed response is completely different, when fault crossing is accounted for. The displacement time histories at the pier top for both sides of the fault resemble the input displacement time histories. However, in “Case B”, the displacements computed at the pier top are consistently larger than the displacements computed at the deck. Hence, it appears that since the deck is continuous over the fault, it tries to “clamp” or hold the substructure (piers) together. Furthermore, the isolation drifts are significantly larger for “Case B” when compared with “Case A”. When fault crossing is accounted for, the isolation systems on both sides of the fault move in opposite directions after an initial half-cycle displacement. That is because the continuous deck is maintaining an “average” or a midline location between the relative ground displacements of the two sides of the fault.

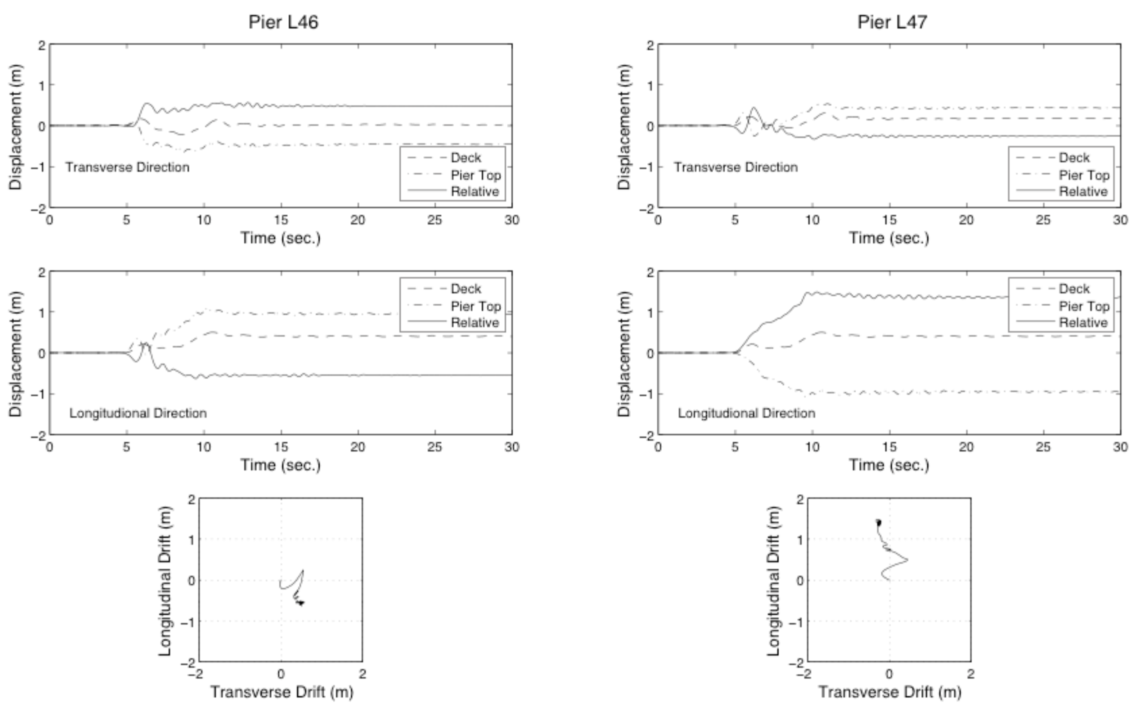

Figure 8. The displacement time histories computed at the deck, pier top and isolation system at Pier 46 and 47 for “Case B” type analysis (accounting for fault crossing).

The importance of accounting for the fault crossing or the “asynchronous” motion between the piers (along with the static fault displacement) is also apparent from the computed isolation demands. For “Case B” the maximum isolation drift demand computed is approximately 1517mm, which is almost twice as much as the demand computed for Case A.

The in-situ observed permanent displacements between the deck and the pier at each pier location where 1000mm longitudinally and 500mm transversely (Rousis et al. 2003). It should also be noted that the bridge deck nearly stopped from falling of the piers by a large number of shear keys at the pier locations. Thus the experienced isolation system drifts would have been much larger than the observed ones if the isolation system had infinite capacity. The calculated demands for the isolation system design appear to be validated by the observed values after the earthquake.

4. CONCLUSIONS

The results of this study demonstrate that the fault crossing of the bridge is manifested as a non-uniform spatial seismic excitation on the structure. This results on additional displacement demands both static and dynamic on the bridge.

AKCNOWLEDGEMENT

The authors would like to thank Dr. Benedikt Halldorsson for his feedback on the high-frequency ground motion simulations and Dr. Marie-Paule Bouin for providing the fault slip model used in the present study.

REFERENCES

ABAQUS (2004). ABAQUS Analysis User's Manual. ABAQUS Inc., Providence, RI.

Akyuz, H. S., R. Hartleb, A. Barka, E. Altunel, G. Sunal, B. Meyer, and R. Armijo (2002). Surface rupture and slip distribution of the 12 November 1999 Duzce earthquake (M 7.1), North Anatolian fault, Bolu, Turkey, *Bull. Seism. Soc. Am.* **92**, 61-66.

Bouin, M.-P., M. Bouchon, H. Karabulut, and M. Aktar (2004). Rupture process of the 1999 November 12 Düzce (Turkey) earthquake deduced from strong motion and Global Positioning System measurements, *Geophys. J. Int.* **159**, 207-211.

Bouchon, M. (1979). Discrete wave-number representation of elastic wave fields in three-space dimensions, *J. Geophys. Res.* **84**, 3609-3614.

Bouchon, M., and K. Aki (1977). Discrete wave-number representation of seismic-source wave fields, *Bull. Seism. Soc. Am.* **67**, 259-277.

Dreger, D., G. Hurtado, A. Chopra, and S. Larsen (2011). Near-field across-fault seismic ground motions, *Bull. Seism. Soc. Am.* **101**, 202-221.

Guney, D., M. Acar, M. T. Ozludemir, and R. N. Celik (2010). Investigation of post-earthquake displacements in viaducts using geodetic and finite element methods, *Natural Hazards and Earth System Sciences* **10**, 2579-2587.

Halldorsson, B., and Papageorgiou, A. S. (2005). Calibration of the specific barrier model to earthquakes of different tectonic regions, *Bull. Seismol. Soc. Am.* **95**, 1276–1300.

Luco, J. E., and J. Anderson (1983). Steady state response of an elastic half-space to a moving dislocation of finite width, *Bull. Seism. Soc. Am.* **73**, 1-22.

Luco, J. E., and R. J. Apsel (1983). On the Green's functions for a layered half-space. Part I, *Bull. Seism. Soc. Am.* **73**, 909-929.

Makris, N., and S.-P. Chang (2000). Effect of viscous, viscoplastic and friction damping on the response of seismic isolated structures, *Earthquake Engrg. Struct. Dyn.* **29**, 85-107.

Mavroeidis, G. P., and A. S. Papageorgiou (2003). A mathematical representation of near-fault ground motions, *Bull. Seism. Soc. Am.* **93**, 1099-1131.

Papageorgiou, A. S., and K. Aki (1983a). A specific barrier model for the quantitative description of inhomogeneous faulting and the prediction of strong ground motion. I. Description of the model, *Bull. Seism. Soc. Am.* **73**, 693-722.

Papageorgiou, A. S., and K. Aki (1983b). A specific barrier model for the quantitative description of inhomogeneous faulting and the prediction of strong ground motion. II. Applications of the model, *Bull. Seism. Soc. Am.* **73**, 953-978.

Park, S. W., H. Ghasemi, J. Shen, P. G. Somerville, W. P. Yen, and M. Yashinsky (2004). Simulation of the seismic performance of the Bolu Viaduct subjected to near-fault ground motions, *Earthquake Engrg. Struct. Dyn.* **33**, 1249-1270.

Pucci, S., D. Pantosti, M. R. Barchi, and N. Palyvos (2007). A complex seismogenic shear zone: The Duzce segment of North Anatolian Fault (Turkey), *Earth Planet. Sci. Lett.* **262**, 185-203.

Roussis, P. C., M. C. Constantinou, M. Erdik, E. Durukal, and M. Dicleli (2003). Assessment of performance of seismic isolation system of Bolu Viaduct, *J. Bridge Eng. – ASCE* **8**, 182-190.

Ucak, A., G. Pekcan, D. Xu, and P. Tsopelas (2007). Demand uncertainties on a seismically isolated multispan bridge due to soil-foundation-structure interaction. 10th World Conference on Seismic Isolation, Energy Dissipation and Active Vibrations, Control of Structure, Istanbul, Turkey, May 2007.

Ugurhan, B., and A. Askan (2010). Stochastic strong ground motion simulation of the 12 November 1999 Duzce (Turkey) earthquake using a dynamic corner frequency approach, *Bull. Seism. Soc. Am.* **100**, 1498-1512.